ELSEVIER

### Contents lists available at ScienceDirect

# Acta Biomaterialia

journal homepage: www.elsevier.com/locate/actbio



# Full length article

# Feasibility evaluation of a Zn-Cu alloy for intrauterine devices: *In vitro* and *in vivo* studies



Guo Bao <sup>a,1</sup>, Kun Wang <sup>a,b,1</sup>, Lijun Yang <sup>a,b,1</sup>, Jialing He <sup>a</sup>, Bin He <sup>a,\*</sup>, Xiaoxue Xu <sup>c,\*</sup>, Yufeng Zheng <sup>d,e,\*\*</sup>

- <sup>a</sup> Department of Reproduction and Physiology, National Research Institute for Family Planning, Beijing 100081, China
- <sup>b</sup> Graduate School of Peking Union Medical College, Beijing 100730, China
- <sup>c</sup> School of Mathematical and Physical Sciences, Faculty of Science, University of Technology Sydney, NSW 2007, Australia
- d School of Materials Science and Engineering, Peking University, No.5 Yi-He-Yuan Road, Hai-Dian District, Beijing 100871, China
- e International Research Organization for Advanced Science and Technology, Kumamoto University, 2-39-1 Kurokami, Chuo-Ku, Kumamoto 860-8555, Japan

#### ARTICLE INFO

#### Article history: Received 19 November 2021 Revised 20 January 2022 Accepted 25 January 2022 Available online 31 January 2022

Keywords: Zn-Cu alloys Copper-containing intrauterine devices Intrauterine microenvironment Biocompatibility Biocorrosion

#### ABSTRACT

The comprehensively adopted copper-containing intrauterine devices (Cu-IUDs) present typical adverse effects such as bleeding and pain at the initial stage of post-implantation. The replacement of Cu material is demanded. Zinc and its alloys, the emerging biodegradable materials, exhibited contraceptive effects since 1969. In this work, we evaluated the feasibility of bulk Zn alloys as IUD active material. Using pure Cu and pure Zn as control groups, we investigated the contraceptive performance of Zn-0.5Cu and Zn-1Cu alloys via *in vitro* and *in vivo* tests. The results showed that the main corrosion product of Zn-Cu alloys is ZnO from both *in vitro* and *in vivo* studies. CaZn<sub>2</sub>(PO<sub>4</sub>)<sub>2</sub>·2H<sub>2</sub>O is formed atop after long-term immersion in simulated uterine fluid, whereas CaCO<sub>3</sub> is generally formed atop after implantation in the rat uterine environment. The cytocompatibility of the Zn-1Cu alloy was significantly higher than that of the pure Zn and pure Cu to the human endometrial epithelial cell lines. Furthermore, the *in vivo* results showed that the Zn-1Cu alloy presented much improved histocompatibility, least damage and the fastest recovery on endometrium structure in comparison to pure Zn, Zn-0.5Cu and pure Cu. The systematic and comparing studies suggest that Zn-1Cu alloy can be considered as a possible candidate for IUD with great biochemical and biocompatible properties as well as high contraceptive effectiveness.

#### Statement of significance

The existing adverse effects with the intrinsic properties of copper materials for copper-containing intrauterine devices (Cu-IUD) are of concerns in their employment. Such as burst release of cupric ions (Cu $^{2+}$ ) at the initial stage of the Cu-IUD. Zinc and its alloys which have been emerging as a potential biodegradable material exhibited contraceptive effects since 1969. In this study, Zn-1Cu alloys displayed significantly improved biocompatibility with human uterus cells and a decreased inflammatory response within the uterus. Therefore, high antifertility efficacy of the Zn-1Cu alloy was well maintained, while the adverse effects are significantly eased, suggesting that the Zn-1Cu alloy is promising for IUD.

© 2022 Acta Materialia Inc. Published by Elsevier Ltd. All rights reserved.

# 1. Introduction

Copper-containing intrauterine device (Cu-IUD) is one of the most widely used contraceptive methods worldwide because of the

great safety, long life span, complete and quick reversibility, and high effectiveness [1]. However, there are some issues associated with the Cu-IUD adoption, such as increased bleeding or pain that occurs immediately after insertion in the uterus and relates to the burst release of Cu<sup>2+</sup> [2,3]. The inflammation in genito-urinary system could be caused from postoperative bacterial infection while placing Cu-IUD during intrauterine surgeries such as caesarean section or induced abortion [4]. High chance of intrauterine infection occurs the first menstrual cycle after insertion of IUD and the highest risk of pelvic inflammation occurs after surgical injuries [5,6].

<sup>\*</sup> Corresponding authors.

<sup>\*\*</sup> Corresponding author at: School of Materials Science and Engineering, Peking University, No.5 Yi-He-Yuan Road, Hai-Dian District, Beijing 100871, China.

E-mail addresses: hebin@nrifp.org.cn (B. He), Xiaoxuehelen.xu@uts.edu.au (X. Xu), yfzheng@pku.edu.cn (Y. Zheng).

<sup>&</sup>lt;sup>1</sup> These authors contributed equally to this work.

Great efforts have been attempted to tackle the problems, changing the shape and size of copper component [7], adding non-steroidal anti-inflammatory drugs [8], or reducing copper grain microstructures [3]. Burst release of Cu<sup>2+</sup> was greatly inhibited while it still exists.

Among the newly developed IUDs containing a variety of active materials, Zn exhibits high potential to be an idea candidate of the active material for IUD. Firstly, Zn<sup>2+</sup> displays high contraception effectiveness owing to the significant suppression of sperm motility by not only bending sperm tail but also inhibiting the anaerobic and aerobic oxidation processes of sperms [9]. Zinc gluconate has been comprehensive adopted as a permanent contraception agent for male dogs and cats via intratesticular administration [10,11]. Zn-bearing IUD was proposed together with Cu-IUD by Zipper et al. in 1969 and tested for contraception in rabbit models [12,13]. Zinc and silver contained IUD were evaluated and compared with Cu contained IUD in 'T' shape in 1974 showing comparable contraceptive efficiency [14]. Zn and ZnO nanoparticles incorporated into the low-density polyethylene (LDPE) nanocomposite were also developed as new type of IUD contraception [15,16]. Furthermore, Zn<sup>2+</sup> also possesses superior bacteriostatic and bactericidal capability [17,18], which might be helpful to prevent or reduce infection risks of reproductive tract while IUD placement [19,20]. For example, Zn-xCu alloys (x = 1, 2, 3,and 4 wt%) could effectively inhibit bacterial adhesion and biofilm formation when it was adopted in vascular stents as biodegradable material [18,21]. Zhou reported that the stents made of Zn-0.8Cu could reduce the adverse effects of vascular pulsation and facilitate better recovery of vessel pulsatility [22]. Moreover, Zn alloys have been developed with required biocompatibility and biodegradation rates in various human body environments for various biomedical applications [23-27]. The corrosion processes of pure Zn were firstly investigated in simulated body fluidic environments [28-31] and the biological molecule' effects within artificial plasma [32,33]. Zn alloys, on the other hand, were thoroughly evaluated from physical microstructures, mechanical properties, biodegradation behaviours and in vivo biocompatibility. For example, Zn-Li-Mn was explored for surgical staples towards gastrointestinal anastomosis [34] and Zn-3Cu for biliary surgery [35]; Zn-Mg alloys [36,37], Zn-Cu-Fe [38] and Zn-Li alloys [39] were developed for cardiovascular stents; Zn-HAP composites [40], Zn-Mn alloys [41] with refined and uniform grains [42], Zn-1.5Mg-Ca/Sr [43], Zn-Sr/Mg alloys [44] and Zn-5 Al-4 Mg [45] were investigated as orthopaedic devices and implants; and Zn-0.1Li and Zn-0.8Mg alloys were preliminarily studied in the intrauterine microenvironment for IUD [46].

With the comprehensive investigations of Zn alloys for a variety of biomedical applications, the feasibility of the Zn alloys as the active materials for IUD has yet been systematically evaluated. In the present study, we chose two Zn-Cu alloys, Zn-0.5Cu and Zn-1Cu to assess their physical, chemical, and biomedical properties as the potential replacement of Cu in IUD. The corrosion behaviours, *in vitro* cytocompatibility, *in vivo* tissue compatibility, and contraceptive efficacy are thoroughly assessed using the pure Cu and pure Zn as control groups.

# 2. Materials and methods

# 2.1. Material preparation

Zn and its two alloys, Zn-0.5Cu and Zn-1Cu (weight percentage, wt%), were prepared from bulk raw materials of high-purity Zn (99.99%) and Cu (99.99%) at the Hunan Rare-Earth Material Research Institute. All the experimental material ingots were homogenized at 350°C for 48 h followed by a water quenching process and subsequently annealed at 260°C for 2 h before extrusion. Extrusion was performed with a reduction ratio of 36:1 at the

squeeze speed of 1 mm/s. Pure copper (99.99%) of 10-mm diameter and 1-m length were purchased from Yuandelai Industrial Materials Co. (Shenzhen, China). The extruded rods were sliced to discs of 10-mm diameter and 2-mm thickness, followed by polishing using silicon carbide (SiC) abrasive papers (Beijing Dongxin Grinding Tools Co. Ltd. China) to obtain granulations from 800 to 2000 grits. The discs were ultrasonically cleaned with ethanol (Beijing Chemical works, China) for 15 min and then air-dried.

# 2.2. Long-term immersion test

The immersion tests were performed according to the method described by ASTM-G31-72 [47] in a simulated uterine fluid (SUF) solution (NaCl 4.97 g/L, KCl 0.224 g/L, CaCl<sub>2</sub> 0.167 g/L, NaHCO<sub>3</sub> 0.25 g/L, glucose 0.50 g/L, and NaH<sub>2</sub>PO<sub>4</sub>·2H<sub>2</sub>O 0.072 g/L) (all chemicals were purchased from Beijing Chemical works, China) at 37°C in a water bath (Tianjin City TAISITE Instrument Co. Ltd., China). The ratio of SUF volume to the Cu exposure surface area was 20 mL/cm<sup>2</sup> and the exposed sample surface area was approximately 2.2 cm<sup>2</sup>. The tests were continued for 300 days. The SUF was refreshed every day from day 1 to day 10, every 5 days from day 11 to day 30, every 15 days from day 31 to day 60, and every 30 days from day 61 to day 300. The pH values of the immersed solutions and the Zn<sup>2+</sup> and Cu<sup>2+</sup> concentrations in the SUFs were monitored and recorded during the 300 days immersion. After 1, 10, 30, 60, 150, and 300 days, five samples were retrieved from the SUF, followed by gentle rinse using distilled water and air drying. Subsequently, the corrosion products on the surface of zinc and copper materials were removed by dipping the samples into chromic acid solution (200 g/L CrO<sub>3</sub>) (Beijing Chemical works, China) for 1 min at 80 °C and then into concentrated sulphuric acid (H2SO4, specific gravity 1.84) (Beijing Chemical works, China) for 3 min at room environment [48]. The degradation rate was determined using the following equation:

$$C = \Delta m/(\rho \times A \times t)$$

where C is the corrosion rate in mm/year,  $\Delta m$  is the weight reduction,  $\rho$  is the density of the material, A is the initial surface area of the disc, and t is the immersion time. At least four measurements were carried out in each group.

# 2.3. Corrosion morphology and product characterizations

The surface morphologies of the long-term immersed Zn, Zn alloys and Cu materials were observed using a scanning electron microscope (SEM) coupled with an energy dispersive spectrometer (EDS) (S-4800 Emission scanning electron microscope, Hitachi). The constituent phases of the corroded product on the surfaces were identified by performing X-ray diffraction analysis (XRD, Rigaku DMAX 2400) under Cu-K $\alpha$  radiation at a scan rate of 4°/min, 40 kV, and 100 mA. The scan range was 10°–90° and 5°–95° for Zn and its alloys and Cu respectively for different immersion time durations. The corresponding chemical species from the XRD results were identified through the peak matching analysis using MDI Jade6 software.

#### 2.4. Electrochemical tests

The electrochemical behaviours of Cu, Zn, Zn-0.5Cu, and Zn-1Cu in the SUF were analysed using an electrochemical workstation (Autolab, Metrohm, Switzerland) at room temperature. A three-electrode cell was used, comprising a saturated calomel electrode (SCE, Tianjin Aida Hengyu Technology Development Co., Ltd., China) as the reference electrode, a platinum counter electrode (Shang Hai Ruosull Technology Co., Ltd., China), and a working

electrode. The exposed area of the specimen in the working electrode was  $0.242~\rm cm^2$ . The stability open circuit potential (OCP) of each specimen was monitored for 1 h. Electrochemical impedance spectroscopy (EIS) was performed within 10 mV perturbation and the measuring frequency ranging from  $10^5~\rm to~10^{-2}$  Hz. The potentiodynamic polarisation tests were performed at a scanning rate of 1 mV/s. The corrosion parameters including OCP, corrosion potential ( $E_{\rm corr}$ ), and corrosion current density ( $i_{\rm corr}$ ) were analysed through a linear fit and Tafel extrapolation to the cathodic and anodic parts of the polarisation curves. All the tests were conducted at least three times to confirm the reproducibility of the results.

#### 2.5. In vitro studies

#### 2.5.1. Cell culture

Human endometrial epithelial cells (HEECs and BNCC354984) and human endometrial stromal cells (HESCs and BNCC267006) were used in this study. The cell lines were purchased from Bnbio Company (Beijing, China). HEESs and HESCs were cultured in Dulbecco's modified eagle medium containing nutrient mixture F-12 (DMEM/F12, Gibco, USA) supplemented with 10% fetal bovine serum (FBS, Gibco, Australia), 100 U/mL penicillin, and 100  $\mu g/mL$  streptomycin (Gibco, USA) in a humidified atmosphere, with 5%  $\rm CO_2$  at 37 °C.

#### 2.5.2. Cell viability assay

The polished experimental samples were washed, air-dried, and then sterilised using ultraviolet radiation for at least 4 h. The samples were incubated in DMEM/F12 medium supplemented with 10% FBS for 24 h and the supernatant was withdrawn and stored at 4 °C until use. The ratio of the samples' exposed-area to the extraction-medium's volume is 1.25 cm²/mL under standard cell culture conditions (a humidified atmosphere, with 5% CO<sub>2</sub> at 37 °C). The pH values of the extracts were measured using a pH meter (PB-10, Sartorius). The Cu²+ and Zn²+ concentration in the extracts was determined using an inductively coupled plasma optical emission spectrometer (ICP-OES, iCAP6300, Thermo). The conventional medium (DMEM/F12 medium supplemented with 10% FBS) was used as the negative control and the culture medium containing 10% dimethyl sulfoxide (Sigma-Aldrich, USA) was used as the positive control.

The cells were seeded in 96-well plates at a density of  $1\times 10^4$  cell/mL (Corning2599, USA), followed by a 24 h incubation for the cell's attachment. The complete culture medium was replaced with 100%, 50% and 10% extracts. The extracts were replaced again on 1, 3, and 5 days before treatment with a normal culture medium to prevent interference. Cell viabilities were determined using the Cell-Counting Kit-8 (CCK-8, Dojindo Molecular Technologies, Japan). CCK-8 solution (10  $\mu$ L) was added to each well of the plate and incubated for 1 h. The spectrophotometric absorbance in each well was measured using a microplate reader (Bio-RAD 680, USA) at 450 nm. Each test was repeated five times.

# 2.6. In vivo studies

# 2.6.1. Animal treatment

Sexually mature female Sprague-Dawley (SD) rats (weight, 190–220 g and age, 8-9 weeks) were obtained from the Charles River Laboratories, China. The animals were acclimatised to the laboratory conditions for 1 week before starting the experiments and were bred under standard conditions. Drinking water and conventional feed were provided *ad libitum*. The protocols for animal care and treatment were approved by the Ethics Committee of the National Research Institute for Family Planning (Issue No. NRIFH200408–1–3). A total of 60 sexually mature female SD rats were randomly divided into five groups (with twelve SD rats in

each group) depending on the implanted materials, namely the sham operation group (SO group), Cu group, Zn group, Zn-0.5Cu group, and Zn-1Cu group. Cu, Zn, Zn-0.5Cu, and Zn-1Cu rods in the diameter of 2 mm and length of 10 mm were prepared. The animals were anaesthetised, and the corresponding material was implanted into their uterine cavity.

# 2.6.2. Histological analysis

The uterine tissues were collected after 3, 7, 14, and 28 days of implantation. The obtained uterine tissue samples were excised into small pieces of 4 mm size, which were immediately fixed in 4% (w/v) paraformaldehyde (Sigma-Aldrich, USA) (pH 7.2) with overnight incubation at 4 °C. The samples were treated using gradient ethanol (70%, 75%, 80%, 95% I and II, 100% I and II) and then immersed in xylene and paraffin. Subsequently, 5-µm thick uterine tissue sections were prepared through microtomy (RM2235, LEICA), which were dewaxed in xylene, rehydrated in decreasing concentrations of ethanol (100% I and II, 95% I and II, 80%, 75%, and 70%), and washed with phosphate-buffered saline. The sections were stained with hematoxylin-eosin (H&E) and then dehydrated using increasing concentrations of ethanol (75%, 95% I and II, 100% I and II) and xylene. The stained specimens were examined, and images were obtained using a high-quality microscope (Olympus CKX41, Olympus Co. Ltd., Tokyo, Japan). Tissues sections were stained with H&E to determine the tissue compatibility, the extent of inflammation, and tissue damage.

### 2.6.3. Antifertility experiment

A total of 50 sexually mature female SD rats were randomly divided into the following five groups: normal control group (NC group) (n=5), SO group (n=5), pure Cu group (n=10), pure Zn group (n=10), Zn-0.5Cu group (n=10), and Zn-1Cu group (n=10). The SD rats were allowed to recover for 15 days before mating. The day on which vaginal plug was observed was designated as day 0.5 of pregnancy. On day 11.5, the animals were sacrificed and the pregnancy outcomes were observed by performing laparotomy and uterotomy.

# 2.6.4. Corrosion morphology characterization for the implanted materials

The implanted materials were removed from three SD rats in each group after 3, 7, 14, and 28 days of insertion. The corrosion morphology and corroded layer product on the surface of the materials were characterized using SEM, EDS, and XRD.

# 2.7. Statistical analysis

Data are expressed as mean  $\pm$  standard deviation (SD). The statistical significance of these data was analysed using the one-way analysis of variance for multiple comparisons, which was followed by the Tukey post hoc tests. P values of <0.05 were considered statistically significant, unless stated otherwise.

# 3. Results

# 3.1. Long-term immersion tests

3.1.1.  $Zn^{2+}$  and  $Cu^{2+}$  release rate and pH value variation of the SUF Fig. 1a presents the release rates of  $Zn^{2+}$  from Zn, Zn-0.5Cu, Zn-1Cu, and  $Cu^{2+}$  from Cu immersed in the SUF over 300 days. The released  $Cu^{2+}$  from the Zn-Cu alloys could be detected for some time point, however, the released amount of  $Cu^{2+}$  was extremely low to the nanograms scale or even out of the detection limit for some time points. Considering the consistent results, we only presented the  $Zn^{2+}$  release rates from the Zn-Cu alloys in this work. From Fig. 1a, it can be seen that the  $Zn^{2+}$  release rates from Zn,

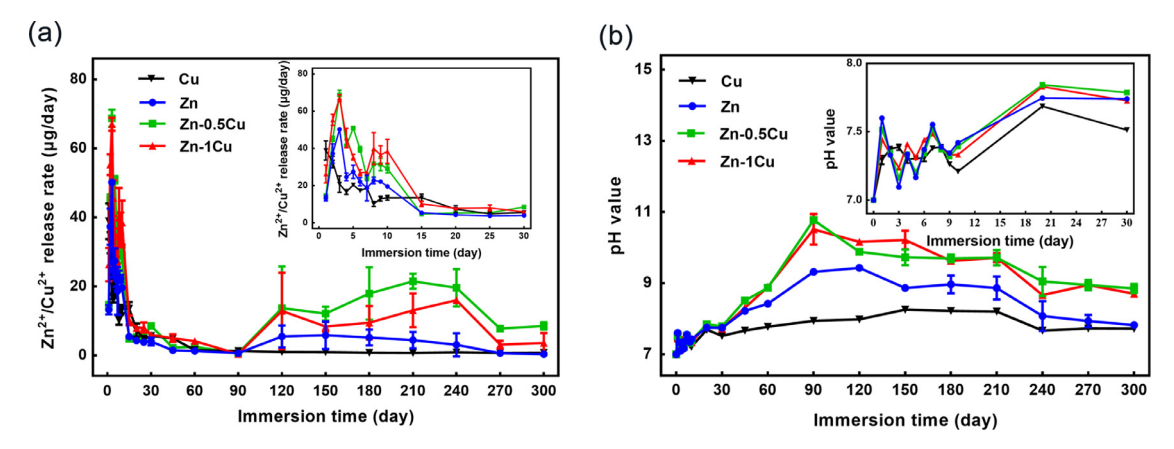


Fig. 1. (a) The release rate of  $Zn^{2+}$  and  $Cu^{2+}$  of Zn, Zn-0.5Cu, Zn-1Cu, and Cu immersed in SUF over 300 days. The line chart represents mean  $\pm$  SD; n=3. (b) pH variations of the SUF immersed with Zn, Zn-0.5Cu, Zn-1Cu, and Cu for 300 days. The line chart represents mean  $\pm$  SD; n=4.

Zn-0.5Cu, and Zn-1Cu groups all exhibited a rapid increase within the first 3 days and a similar fast decrease in the next 5 days. The maximum Zn<sup>2+</sup> release rates from Zn, Zn-0.5Cu and Zn-1Cu were 50.20  $\mu g/day$ , 68.73  $\mu g/day$  and 67.02  $\mu g/day$  respectively. After a small increase from 8th day to 10th day, the Zn<sup>2+</sup> release rates of the three Zn materials decreased to a very low level (5.40  $\mu g/day$ ) after 15 days' immersion and continued decreasing until 90 days at a quite close release rate of 0.38  $\mu g/day$ . Afterwards, the Zn, Zn-0.5Cu and Zn-1Cu exhibited a slight increase in the Zn<sup>2+</sup> release rate. Comparing the overall Zn<sup>2+</sup> release rates during the entire immersion process, Zn<sup>2+</sup> from Zn-Cu alloys was higher than that from Zn. On the other hand, Cu material exhibited a typical burst release of Cu<sup>2+</sup> within initial 10 days from 38.91  $\mu g/day$  to 13.47  $\mu g/day$  followed by the decreased release rate up to 25 days and thereafter a steadily low Cu<sup>2+</sup> release rate at 0.72  $\mu g/day$  until 300 days

The pH values of the SUFs were measured and recorded throughout the 300 days of the immersion and are shown in Fig. 1b. The pH values of the SUFs immersed with Zn materials showed upward trend from day 1 to day 30 with significant fluctuations in first 10 days within the range of 7.0 to 7.6. The pH value of the Zn-Cu alloys then increased to approximately 10.5 on day 90 when the Zn<sup>2+</sup> release rates reached to the lowest level and eventually decreased to approximately 9.0 on day 300. While the pH value of the SUF immersed with pure Zn presented the similar trend with relatively slight fluctuations, it decreased from 9.0 to 8.0 during 300 days of immersion. The pH value of the SUF with Cu showed an increase in the early stage and maintained about a stable pH of 8.0 after a month.

# 3.1.2. Morphological characterization, corrosion product, and corrosion rates

Fig. 2 exhibits the corrosion rates of pure Zn, Zn-0.5Cu, Zn-1Cu, and pure Cu immersed in the SUF for 300 days. All metallic materials showed highest corrosion rates in the beginning of immersion, on the first day. Pure Zn corroded at the relative low rate around 0.03 mm/year since the 10th day immersion until 150th day and at even lower rate around 0.01 mm/year until 300 days. Both the Zn-0.5Cu and Zn-1Cu exhibited a sharp drop of the corrosion rates from 1 day to 10 days immersion, then the corrosion rates presented increasing trend afterwards until 300 days' immersion. On the other hand, pure Cu displayed continuously decreased corrosion rate in SUF over the 300 days from 0.13 mm/year to 0.01 mm/year. In the first 10 days, the corrosion rate of pure Cu was significantly higher (P < 0.01) than that of Zn and its alloys. While from 30 days' immersion onwards, the corrosion rates of Zn-Cu al-

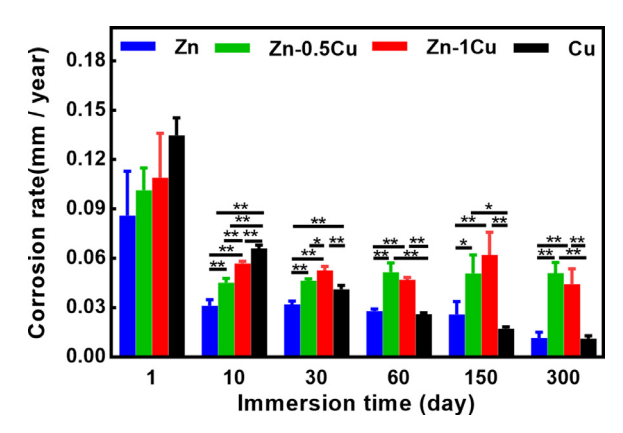


**Fig. 2.** Corrosion rates calculated from the weight loss for the Zn, Zn-0.5Cu, Zn-1Cu, and Cu immersed in SUF for 1, 10, 30, 60, 150, and 300 days. The bar graph represents mean  $\pm$  SD; n = 4; \*P < 0.05 and \*\*P < 0.01.

loy were significantly higher (P < 0.01) than that of pure Cu and pure Zn.

The corrosion processes of the metallic materials were investigated from the corrosion morphology observation after immersion in the SUF for different days. Fig. 3 is the SEM images showing the typical morphologies of the materials' surfaces. After 1 day of immersion, local pitting was observed on the surface in the Zn, Zn-0.5Cu, and Zn-1Cu groups while pure Cu surface was fully covered with a porous layer of corrosion product. After 10 days of immersion, the corrosion products were locally formed at the corrosion pits areas and the corrosion pits were more pronounced on the surface of the Zn and alloys. Considerably large sized corrosion product in the shape of spiky spheres could be found on the pure Zn surface while much more spheres could be observed from Zn-0.5Cu surface and quite dense corrosion produces in a variety of sizes covered on the surface of Zn-1Cu. Pure Cu surface after 10 days' immersion in SUF presented crystal corrosion products in relatively uniform size covering the whole surface. With the prolonged immersion time to 30 days and afterwards, the spiky corrosion products on pure Zn surfaces were increased in size and density to the whole view suggesting the corrosion was occurred on the whole surface. While the corrosion products on both Zn alloys were gradually increased in dimensions to fully cover the surfaces with various morphologies. In comparison to the Zn and Zn alloys, pure Cu surface formed corrosion products uniformly on the whole surface area and in relatively smaller size. After 300 days immersion, pure Cu surface was covered densely with solid microspheres, while the surfaces of Zn, Zn-0.5Cu and Zn-1Cu still pre-

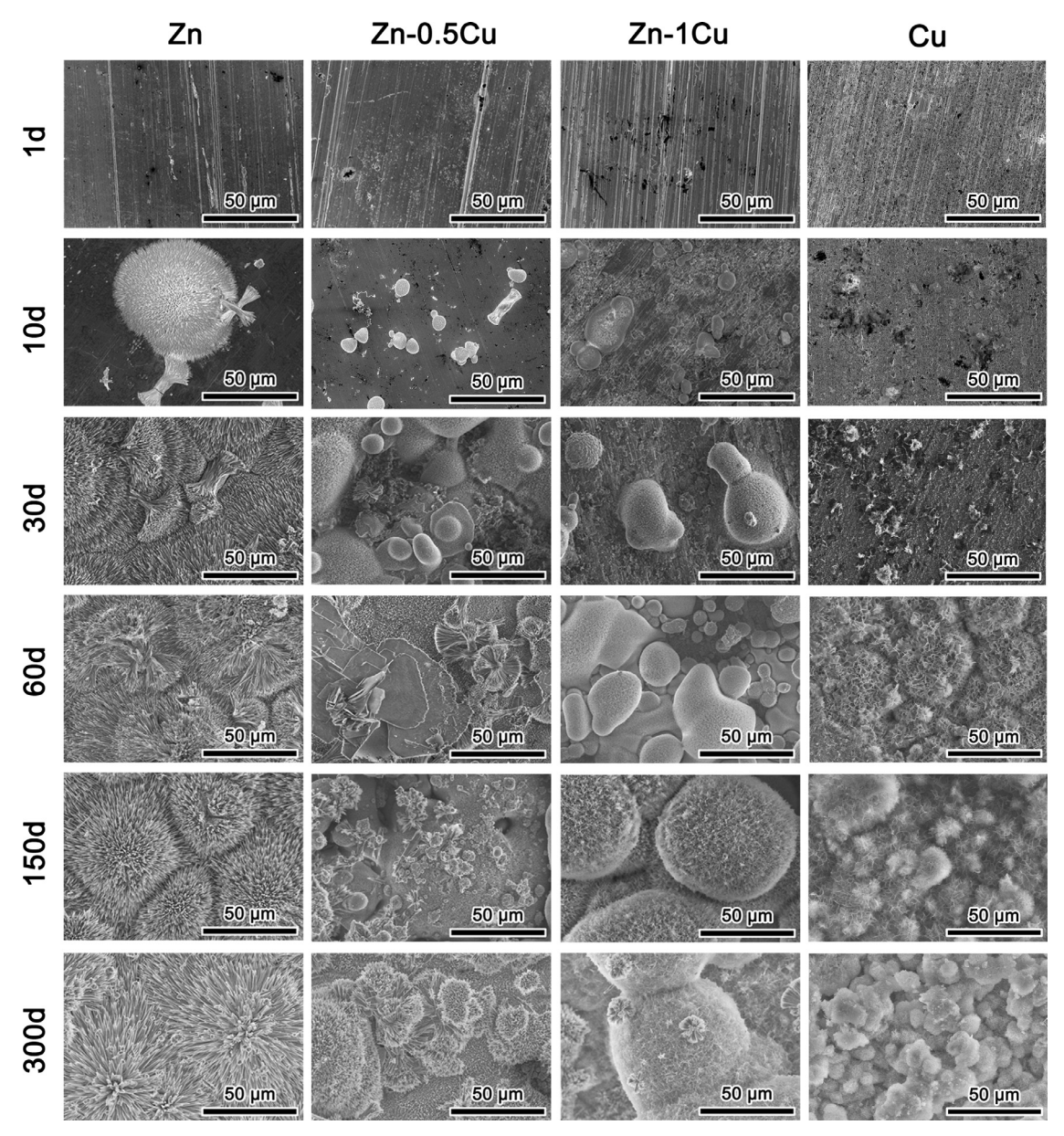


Fig. 3. Corrosion morphologies of Zn, Zn-0.5Cu, Zn-1Cu and Cu immersed in the SUF for 1, 10, 30, 60, 150, and 300 days.

sented very porous, spikey and large microspheres, suggesting the corrosion product layer was very packet on Cu and quite loose corrosion product layer on Zn and Zn alloys.

The EDS results were revealed in Fig. S1 for the four materials immersed in SUF for 10 days and 300 days respectively. The elements of Zn, Ca, O, P, and C were detected in the corrosion products of Zn and its alloys since 10 days' immersion. The corrosion products of Zn and Zn-0.5Cu samples were found to contain C, Zn, O, P, and Ca. There was no observed difference in the composition elements from the short- and long-term immersion. On pure Cu surface, the majority element detected were Cu and O for the short time immersion while Ca, P, Cl, and C elements showed up with Cu and O after immersed in SUF for 300 days.

The phase compositions of the corrosion products of Zn, Zn-0.5Cu, Zn-1Cu, and Cu immersed in SUF for a series of time period were characterized using XRD and shown in Fig. 4. It can be seen that the corrosion products were not very detectable for 1-day immersion for Zn and Zn alloys, although the ZnO peaks presented slightly with Zn patterns. CuZn<sub>5</sub> was found as the orig-

inal Zn alloy phase from both Zn-0.5Cu and Zn-1Cu. From 10 days' immersion, ZnO and  $CaZn_2(PO_4)_2 \cdot 2H_2O$  were identified as the main corrosion products for all Zn materials. On the contrary,  $Cu_2O$  was relatively obvious from one day immersion for pure Cu material in SUF, which agrees well with the corrosion morphology observation of Cu presenting uniformly covered corrosion product on day 1 (Fig. 3).  $Cu_2O$  was the only corrosion product from XRD characterization, suggesting that the minority elements detected from EDS (Fig. S1) could be from the amorphous phases.

#### 3.2. Electrochemical measurements

The OCPs of four materials during 3600 s of immersion in SUF were recorded and shown in Fig. 5a. The OCP of pure Cu was stabilized at about -0.19 V presenting the highest potential compared with the pure Zn and its alloys. Additionally, the OCPs of Zn-0.5ZCu and Zn-1Cu alloys present a higher potential compared with pure Zn. Fig. 5b presents the potentiodynamic polarisation test results

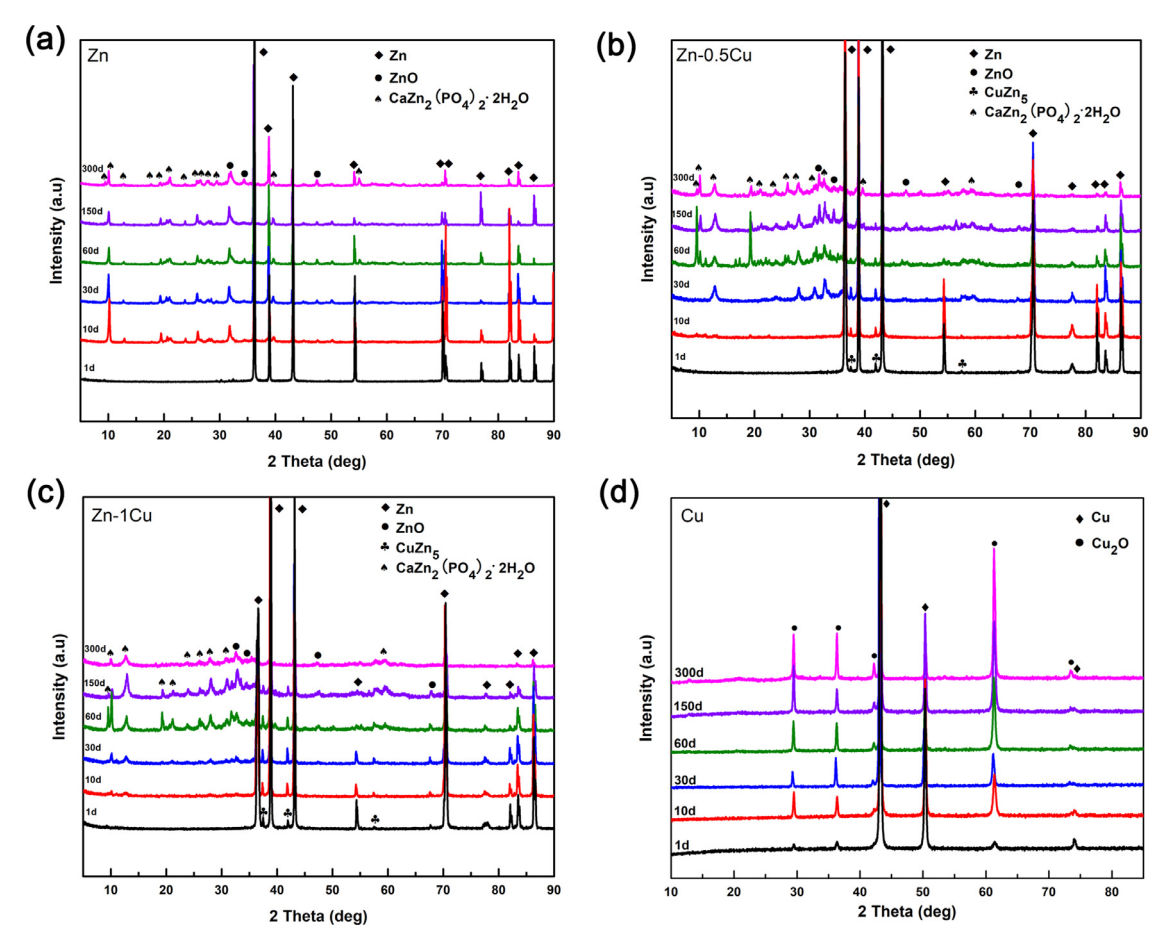


Fig. 4. XRD patterns of (a) Zn, (b) Zn-05Cu, (c) Zn-1Cu and (d) Cu immersed in the SUF for 1, 10, 30, 60, 150, and 300 days.

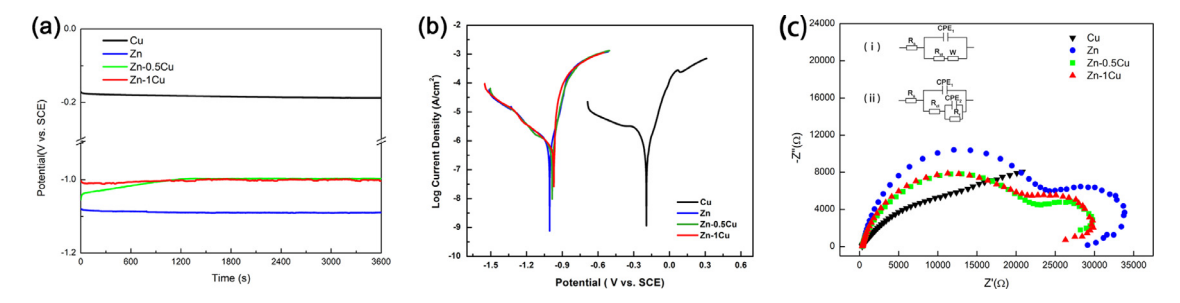


Fig. 5. The open circuit potential plots, potentiodynamic polarisation curves and the electrochemical impedance spectra with the electric equivalent circuits of Zn, Zn-0.5Cu, Zn-1Cu and Cu in the SUF.

**Table 1** The parameters of open circuit potential,  $E_{corr}$ ,  $i_{corr}$ ,  $i_{corr}$ , and corrosion rates of Zn, Zn-0.5Cu, Zn-1Cu and Cu in the SUF. \* P < 0.05 when compared with the Zn.

Materials	i <sub>corr</sub> (μA/cm <sup>2</sup> )	E <sub>corr</sub> (V)	Corrosion rate (mm/year)
Zn	2.1±0.1	-0.95±0.03	0.031±0.001
Zn-0.5Cu	3.0±0.2*	-0.95±0.05	0.044±0.003*
Zn-1Cu	3.5±0.2*	-0.96±0.04	0.052±0.003*
Cu	3.5±0.2*	-0.20±0.01*	0.041±0.003*

for the four materials in the SUF and the obtained electrochemical corrosion current and potential values are listed in Table 1. There was no significant difference (P>0.05) in corrosion potentials among three Zn materials. However, both the corrosion current density and corrosion rate of pure Zn, 2.12  $\mu$ A/cm² and 0.03

mm/year were significantly lower than those of the Zn alloys (P < 0.05). Further comparisons in the two parameters of Zn-0.5Cu and Zn-1Cu did not show significant variations (P > 0.05), 2.95 µA/cm² and 3.51 µA/cm². Zn-1Cu exhibited the highest corrosion current density. Pure Cu presents the highest corrosion potential compared with Zn and its alloys (P < 0.05). Moreover, both the corrosion current density and corrosion rate of pure Cu, 3.52 µA/cm² and 0.04 mm/year were significantly higher than those of pure Zn (P < 0.05). The EIS spectra of Cu, Zn, Zn-0.5Cu, and Zn-1Cu exposed to SUF are shown in Fig. 5c and the fitting results are listed in Table 2. The Nyquist plot of Cu presents the incomplete capacitive resistance arc. It clearly shows that the curvature radius of the Cu sample is larger than that of the Zn, Zn-0.5Cu, and Zn-1Cu samples, suggesting the highest charge-transfer resistance of the Cu sample and thus higher corrosion resistance of Cu comparing to Zn and its

**Table 2**The fitted results of the electrochemical impedance spectra of Cu, Zn, Zn-0.5Cu, and Zn-1Cu.

	$R_s \; (\Omega cm^2)$	R <sub>ct</sub> (Ωcm <sup>2</sup> )	$R_f (\Omega cm^2)$	$CPE_1 (\Omega^{-1} s^n cm^{-2})$	N	$\text{CPE}_2 \ (\Omega^{-1} \text{s}^{\text{n}} \text{cm}^{-2})$	n	W ( $\Omega^{-1}$ s <sup>n</sup> cm <sup>-2</sup> )
Cu	71.3	4385.0	-	1.83E-04	0.57	-	-	8.42E-05
Zn	90.9	6159.9	1768.1	4.78E-06	0.86	2.94E-04	1.08	-
Zn-0.5Cu	84.8	6676.8	3115.8	5.06E-06	0.82	3.10E-04	0.89	-
Zn-1Cu	84.9	4864.4	2323.9	5.43E-06	0.82	1.87E-04	0.78	-

alloys. The corresponding electrical equivalent circuit (EEC) of Cu in the SUF was shown as Fig. 5c (i). R<sub>s</sub> is identical to the electrolyte resistance, the constant phase element (CPE<sub>1</sub>) is almost like Warburg impedance when the n value is close to 0.5 while the presence of the Warburg (W) impedance indicates that the mass transport is limited by the formed oxide layer on the Cu surface. The EIS responses of Zn and its alloys characteristically appeared two semicircle-like curves (Fig. 5c) which corresponded to two time constants, mainly one high frequency and one low frequency capacitance loop. The model (ii) was used to interpret the result for Zn and Zn alloys. The semicircle in the high frequency region is related to the corrosion products formed in the uniformly corroded region of the sample surface and corresponds to the R<sub>ct</sub> and CPE<sub>1</sub> in the EEC model (ii) referring to the charge transfer resistance and the electric layer at the interface of substrate and electrolyte. The semicircle in the low frequency region, corresponding to the R<sub>f</sub> and CPE2, is related to interfacial charge transfer processes and electrochemical double-layer effects at the sample/electrolyte interface. The semicircle diameter of Zn-0.5Cu and Zn-1Cu are smaller than that of pure Zn, indicating that its corrosion resistance is reduced.

#### 3.3. In vitro cytocompatibility studies

Variations in the pH of the cell culture media in the presence of the three material extracts were monitored, and the results are presented in Fig. S2 No difference was observed between the pH values of the test materials before and after immersion.

The cytotoxicity evaluation results for 100%, 50%, and 10% extracts of Zn, Zn-0.5Cu, Zn-1Cu, and Cu are presented in Fig. 6 According to the International Organization of Standardization (10993-5:2009 Biological evaluation of medical devices-Part 5: Tests for in vitro cytotoxicity), cell viability higher than 75% is considered as acceptable cytotoxicity for biomedical devices. It can be seen from Fig. 6 that the cell viabilities of HEECs cultured in the 100% extracts of all four metallic materials for 1, 3 and 5 days were very low and the highest one was 62% from the 100% extracts of Zn-1Cu for 5 days' culture. All Zn materials presented better HEEC cell viability than the pure Cu. It is worthy to note that Zn-0.5Cu exhibited lowest cell viability among the Cu, Cu-0.5Zn and Zn-1Cu. Similar scenario occurred for the cell viabilities of HESCs cultured in the 100% extracts of all four metallic materials for 1, 3 and 5 days. Cu exhibited much lower cell viability than the Zn and the alloys. The Zn-0.5Cu exhibited slightly higher level cell viability than Cu, however, it was much lower than pure Zn and Zu-1Cu. Both pure Zn and Zn-1Cu presented much higher cell viability of the HESCs than that of the HEECs. The highest cell viability (110%) was from the 100% extract of Zn-1Cu cultured for 5 days. Furthermore, the 50% and 10% extracts of Zn, Zn-0.5Cu, and Zn-1Cu exhibited no cytotoxicity to both HESCs and HEECs, whereas 50% and 10% extracts of Cu exhibited severe cytotoxicity to both cells cultured for 1 day.

The measured concentrations of  $Zn^{2+}$  and  $Cu^{2+}$  in the 100% extract of Zn, Zn-0.5Cu, Zn-1Cu and Cu were listed in Table 3. There was no considerable difference in  $Zn^{2+}$  or  $Cu^{2+}$  concentrations ob-

**Table 3** Ion concentrations of Zn, Zn-0.5Cu, Zn-1Cu and Cu immersed in the culture medium (DMEM/F12 + 10% FBS + 100 U·mL<sup>-1</sup> penicillin and 100 g·mL<sup>-1</sup> streptomycin) for 24 h (mean  $\pm$ SD; n = 3).

Materials	Zn ( $\mu$ g/mL)	Cu (ng/mL)
Before extraction	0.5±0.1	15.4±0.7
Pure Zn	15.4±1.0	-
Zn-0.5Cu alloy	17.7±1.8	17.5±0.7
Zn-1Cu alloy	$16.3 \pm 0.9$	$21.4 \pm 0.4$
Pure Cu	-	130.1 $\pm$ 5.6 ( $\mu$ g/mL)

served among Zn materials, but Cu released 130.13  $\mu g/mL$  Cu<sup>2+</sup> which was about 10 times higher than the Zn<sup>2+</sup> from pure Zn.

#### 3.4. In vivo implantation test

### 3.4.1. Histological observations

To evaluate tissue compatibility of Zn, Zn-0.5Cu, Zn-1Cu, and Cu with the endometrium, samples in the rod shape were implanted into the rat uterine cavity. Histologic examination of the endometrial tissues that directly contacted and interacted with the inserted rod samples for 3, 7, 14 and 28 days are presented in Fig. 7. The insets show the uterine cross sections and the enlarged images are the squared area in the insets. The endometrial cells of the rats in the SO group exhibited clear outlines, normal gland numbers, complete glandular epithelium, and slight inflammatory reaction after surgery. There were no changes along the increased time. Conversely, after 3 days of implantation, strong tissue reactions were observed in the Zn, Zn-0.5Cu, Zn-1Cu, and Cu groups. With the implantation of Zn, Zn-0.5Cu, Zn-1Cu, and Cu materials for 3 days, the endometrial structures were severely damaged, which was evident from the disordered arrangement of endometrial stromal cells (the area shown using red arrows in the enlarged images), exudation of inflammatory cells in the uterine cavity (black arrows in the insets images), structural damage to the glands, and structural disintegrity of the epithelial cells. In addition, obvious inflammatory cells were found infiltrating into the endometrial tissues after implantation of the four groups of materials, which suggested the occurrence of inflammatory reaction after implantation of the materials. Overall, the tissue reactions in the Zn-1Cu group were milder than those in the Zn, Zn-0.5Cu, and

After implanted for 7 days, the endometrial tissues interacted with the four metallic rods still showed aggravated damages in the endometrial structures and the inflammatory cell infiltration in the tissues. The exudation of inflammatory cells in the uterine cavity could be observed in the tissues interacted with pure Zn, Zn-0.5Cu, and Cu. The endometrial structure directly contacted with Zn-0.5Cu and Cu rod presented further damage with obvious tissue separation. It is worth to note that the endometrial stromal cell structure was considerably improved from the endometrial tissue contacted with Zn-1Cu for 7 days although the overall tissue conditions were similar to the tissues of pure Zn and Zn-0.5Cu. Therefore, the endometrial structure displayed a self-repair tendency with the implantation of Zn-1Cu. The pure Cu still caused

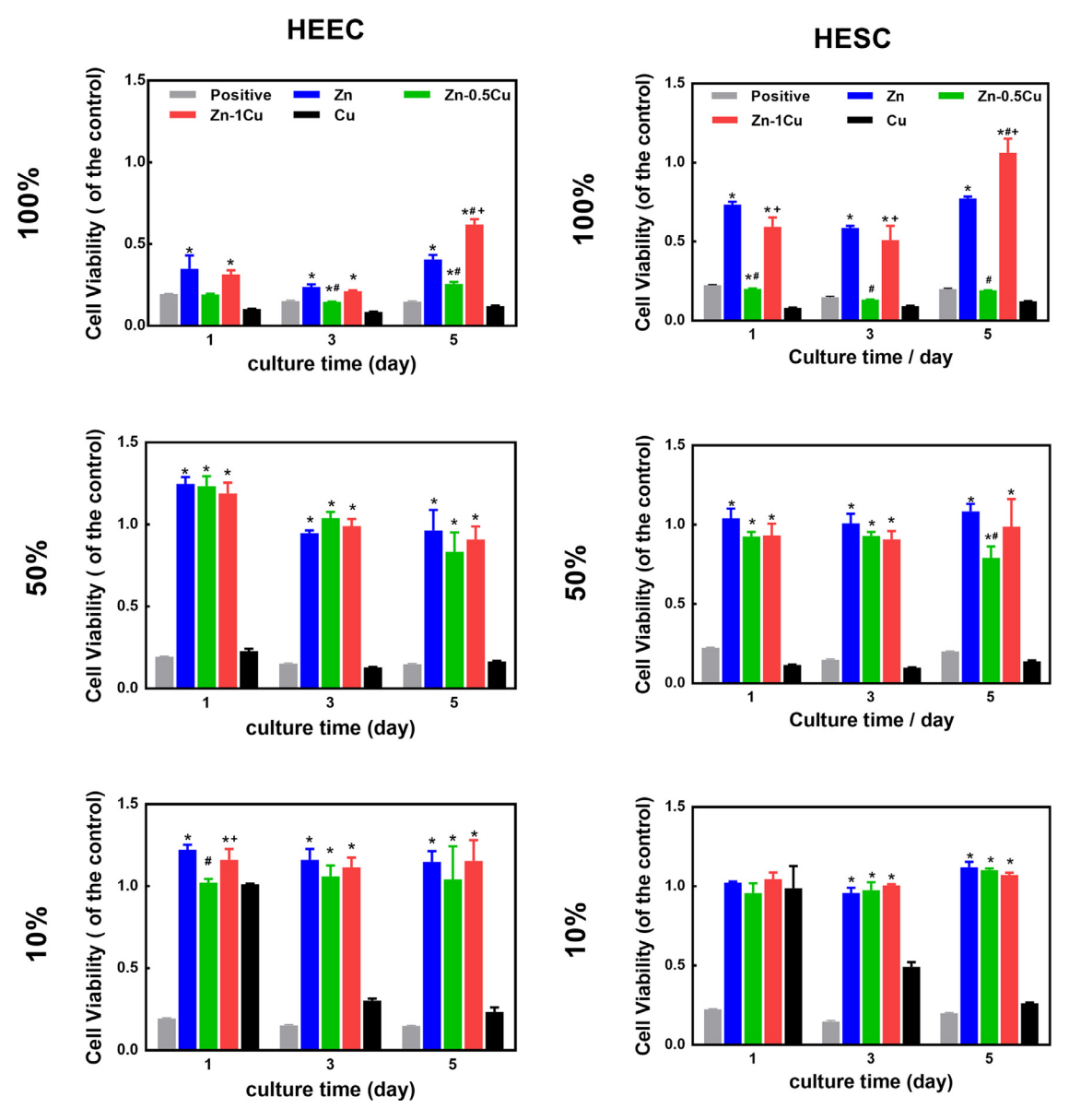


**Fig. 6.** Viabilities of HEECs and HESCs after 1, 3, and 5 days of incubation in the 1005, 50% and 10% extracts of Zn, Zn-0.5Cu, Zn-1Cu and Cu in SUF, normal medium, and normal (negative control) with 10% DMSO (positive control). The bar graph represents mean  $\pm$  SD; n = 5, \*P < 0.05; each time point and Zn, Zn-0.5Cu, and Zn-1Cu groups compared with the Cu group; # P < 0.05, each time points and the Zn-Cu group compared with the Zn group; + P < 0.05 the Zn-1Cu group compared with the Zn-0.5Cu group.

disordered endometrial stromal cells in the endometrial tissue after 7 days' implantation.

After 14 days' implantation, the endometrial tissue structure inserted with Zn-1Cu exhibited obvious repaired tissue with restored stromal cell morphology, reduced inflammatory cells infiltrated by tissues, and zero intrauterine exudate. However, for the endometrial structures implanted with the Zn-0.5Cu and pure Cu, the intrauterine exudate and tissue separation were persistently presented without self-repair tendency. Pure Cu still present a lot of exudations of inflammatory cells in the uterine cavity.

After the Zn-1Cu implanted for 28 days, the overall structure of the endometrium recovered completely with orderly arranged endometrial stromal cells showing clear contour and no inflammatory reaction while the glandular epithelial structure was not fully recovered. The endometrial structures implanted with other three materials, Zn, Zn-0.5Cu, and Cu also showed self-repair at different extent after 28 days. For the pure Zn, the endometrial epithelial cell structure was restored to integrity, and the intrauterine exu-

date disappeared. However, local inflammatory cell infiltration and stromal cell disordered arrangement could still be observed. For Zn-0.5Cu and Cu, the endometrial stromal cells displayed slight ordered arrangement. However, a part of the shed tissue and inflammatory cells could still be seen in the uterine cavity. It can be seen that the Zn-1Cu displayed the highest compatibility with uterine tissue.

# 3.4.2. Antifertility effectiveness

The antifertility experiment performed using rat model presented the results in Table 4. No embryos were observed in the uterine horns where the materials were implanted, whereas normal embryos were found in the contralateral uterine horns of all rats as well as bilateral uterine horns of the NC and SO groups. Antifertility rates for the rats implanted with Zn, Zn-0.5Cu, and Zn-1Cu were all 100% similar to those with Cu material, suggesting that the antifertility efficacy of Zn, Zn-0.5Cu, and Zn-1Cu is comparable to that of Cu materials.

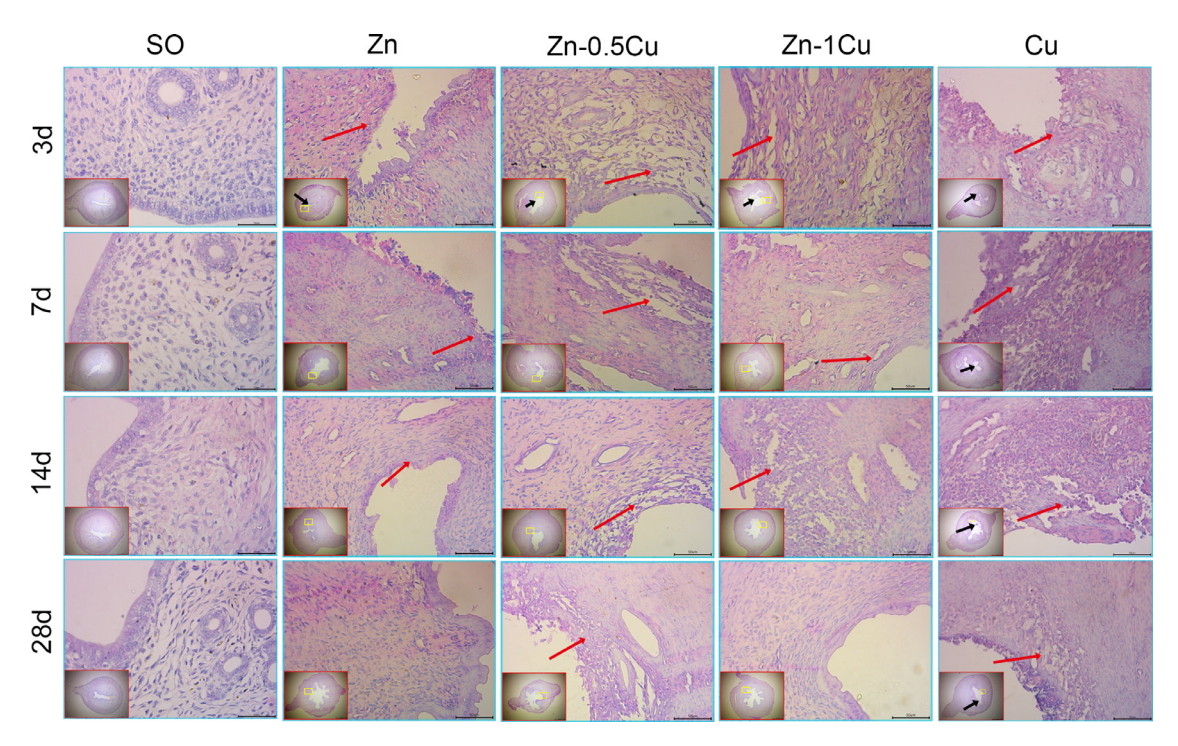


Fig. 7. Histological images of the haematoxylin-eosin-stained Sprague-Dawley rat uterine tissues from the Zn, Zn-0.5Cu, Zn-1Cu and Cu materials after implantation in rate uterine cavity for 3, 7, 14, and 28 days.

**Table 4** Antifertility results of the Zn, Zn-0.5Cu, Zn-1Cu and Cu materials. \* P < 0.05 when compared with the negative group.

Group	n	No. of embryos in material-bearing uterine horn $(\bar{x}\pm SD)$	No. of embryos in contralateral uterine horn $(\bar{x}\pm SD)$	No. of pregnant animals	Antifertility rate (%)
NC	5	7.4±1.4	6.0±1.9	5	0
SO	5	5.3±1.2	5.7±0.9	5	0
Cu	10	0	6.8±0.8	0	100*
Zn	10	0	7.8±1.3	0	100*
Zn-0.5Cu	10	0	7.0±2.9	0	100*
Zn-1Cu	10	0	5.0±0.6	0	100*

# 3.5. Post characterizations of the implanted Zn and Cu materials

# 3.5.1. Corrosion morphology

The surface corrosion morphology of the Cu, Zn, Zn-0.5Cu, and Zn-1Cu materials were observed after these materials were implanted into the rats' uterine cavity for 3, 7, 14, and 28 days, and the results are presented in Fig. 8. The SEM images showed gradually increased corrosion product layers on the surface of the implanted Cu, Zn, Zn-0.5Cu, and Zn-1Cu rods with the increase in the implantation period. The corrosion products on the surface of pure Zn and Zn alloys formed locally adjacent to the corrosion pits first and gradually connected together to cover the whole surface, so the surfaces of the corrosion product layer fluctuated. On the other hand, the uniform corrosion occurred on the surface of pure Cu that the corrosion product layer was also uniformly covered the surface and peeled-off areas on the surface were also quite even.

Fig. S3 shows the EDS analysis on the corrosion products of the four metallic materials after these were inserted to the rats' uterine cavity for 3, 7, 14, and 28 days. In the early stage of implantation, the corrosion products on the surface of pure Zn mainly contained C, N, O, Zn, and P. The corrosion products on Zn-0.5Cu and Zn-1Cu surfaces mainly contained C, N, O, Zn, P, S, and Ca. EDS results in the later stage of implantation revealed that the corrosion product elements on the surface of the three groups of materials contained C, N, O, Zn, P, S, and Ca. Compared with the elemental analysis results of the *in vitro* immersion experiment, elements N and S were

detected on the surface of the Zn and Cu materials implanted in the uterine cavity of the rats, suggesting that in addition to the oxides on the surface of the Zn and Cu materials, some uterine tissues or organic matter were deposited on the surface of the materials.

# 3.5.2. Composition of corrosion products

The XRD patterns in Fig. 9 show the phase constitutions of the corrosion products on the surface of the materials after their implantation in the uterine cavity of rats for different periods. Compounds such as  $\text{Cu}_2\text{O}$ ,  $\text{Cu}_0$ ,  $\text{Cu}_2\text{S}$ , and  $\text{CaCO}_3$  were observed within 3 days of implantation. With the increase in implantation time, the amount of  $\text{Cu}_2\text{O}$  deposited on the surface also increased. The main corrosion products in the Zn, Zn-0.5Cu, and Zn-1Cu materials were ZnO, Zn(OH)<sub>2</sub>, and CaCO<sub>3</sub>.

# 4. Discussion

Zn has been identified with contraceptive effectiveness in the previous work [49] by comparing the pure Cu with Cu-Zn alloys, Cu-38Zn and H62 alloy, as the active materials in the Cu-IUD. The key findings that Cu-Zn alloys exhibited comparable contraceptive effectiveness but much reduced burst release of Cu<sup>2+</sup>, less cytotoxicity and greatly improved tissue compatibility with much smoother corrosion surface suggested Zn and Zn alloys could be a new contraceptive metallic materials. In this work, we carried

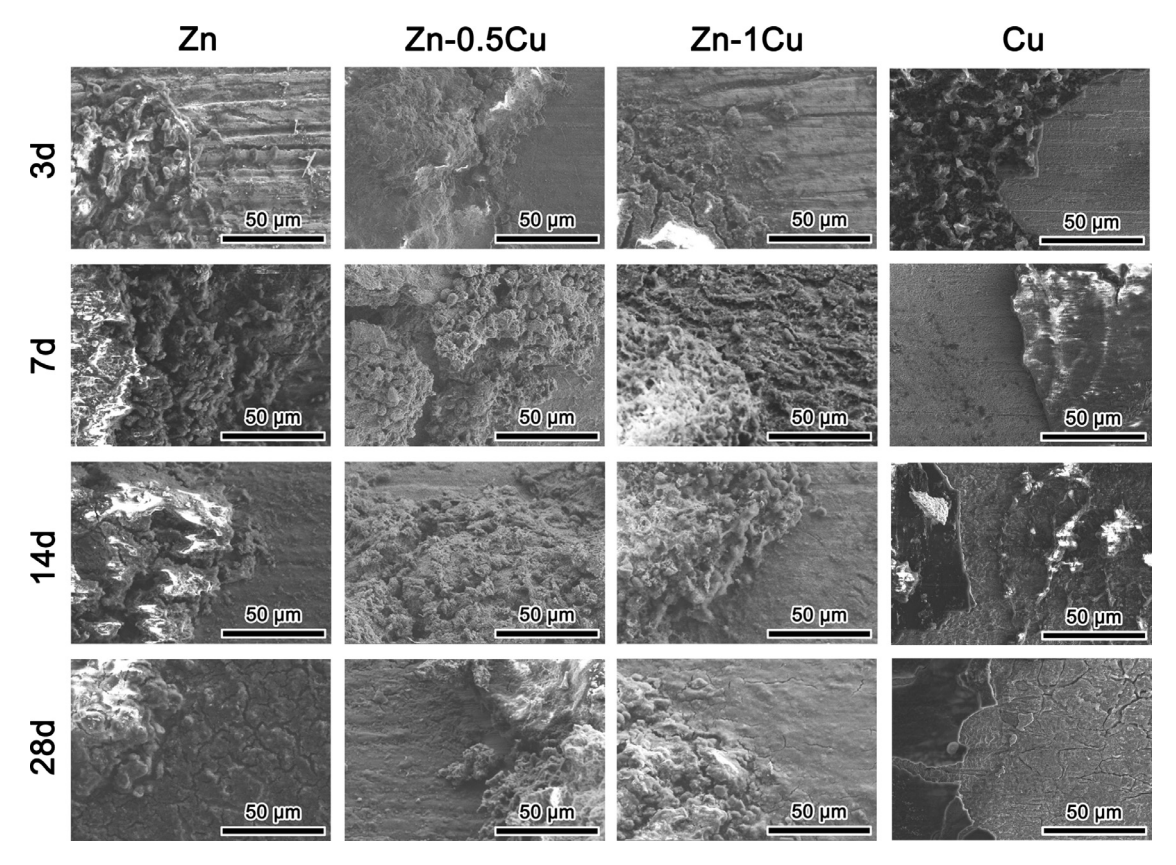


Fig. 8. Corrosion morphologies of Zn, Zn-0.5Cu, Zn-1Cu and Cu materials after implantation in rate uterine cavity for 3, 7, 14 and 28 days.

out the systematic evaluation on the pure Zn and Zn alloys and the results demonstrated that the Zn and Zn alloys could be the potential replacement of Cu in IUD, especially the Zn-1Cu exhibiting the best biocompatibility and excellent contraceptive efficiency. The working mechanism for Zn and alloys as the active materials for IUD is discussed here in biocorrosion behaviour, biocompatibility aspects for the feasibility of the Zn-Cu alloy as an IUD active material.

# 4.1. Degradation behaviours of Zn-Cu alloys in the uterine microenvironment

The Zn and its alloys degrade in a similar manner with the reported investigations in neutral or alkaline solutions [30,50] that Zn-based alloys undergoes oxygen-absorbing corrosion via the anodic oxidation of Zn and cathodic reduction of oxygen. The reactions can be presented as Eq. (1) and Eq. (2), respectively [31]. Therefore, when Zn and its alloys were immersed in the SUF at pH of 7.0, Zn starts to dissolved to  $Zn^{2+}$  and  $OH^-$  and accumulates in the solution, thus the pH value of the SUF would increase rapidly, as Fig. 1b shows the initial increase for Zn, Zn-0.5Cu, and Zn-1Cu alloys. With the progression of the reaction, the corrosion passivation films of ZnO and  $Zn(OH)_2$  gradually form through the reactions the  $Zn^{2+}$  and  $OH^-$  and the pH value of the solution would decrease in the later stage as shown in Fig. 1b. The chemical reactions are represented by Eqs. (3) and (4) [31].

$$Zn(s) \to Zn^{2+}(aq) + 2e^{-}$$
 (1)

$$2H_2O + O_2 + 4e^- - \to 4OH^- - \tag{2}$$

$$Zn^{2+} + 2OH^{-} - \rightarrow Zn(OH)_{2}$$
 (3)

$$Zn^{2+} + 20H^{-} \rightarrow ZnO + H_2O$$
 (4)

With the prolonged immersion time (10 days or longer) of Zn alloys in SUF, a new product can be formed, CaZn<sub>2</sub>(PO<sub>4</sub>)<sub>2</sub>·2H<sub>2</sub>O (Figs. 4 and 5), which is consistent with the previous report for Zn-0.1Li and Zn-0.8Mg alloys [46]. The later formed corrosion product could originate from the reaction of the Zn(OH)<sub>2</sub> and the Ca<sup>2+</sup> and PO<sub>4</sub><sup>3-</sup> in SUF and formed more stable CaZn<sub>2</sub>(PO<sub>4</sub>)<sub>2</sub>·2H<sub>2</sub>O on the surface of Zn in the spiky and porous morphology. The porous structures provided channels for the SUF to diffuse to Zn surface, which enables the continuously steady or even increased corrosion rate in the later stage of the long-term immersion (Fig. 1a) when the corrosion products thicken and fully covers the surface. Moreover, with the decreased corrosion rate (Fig. 2), the corresponding cathodic reaction weakened and the generation of hydroxide decreased, whereas the constantly formed corrosion products consumed OH- in the solution, which may have led to a decrease in the pH value of the solution.

When the Zn and its alloys are implanted in the biological environments, like rats' uterus, the corrosion processes are quite similar to the *in vitro* tests. The uneven and rolling surfaces with locally formed corrosion products of all the Zn materials implanted for up to 30 days. The corrosion products are not in the shape of spiky sphere but still very porous. However, the corrosion products are mainly ZnO, CaCO<sub>3</sub> and Zn(OH)<sub>2</sub> on the surface of the Zn materials [43]. Therefore, in a dynamic *in vivo* environment like rat uterine microenvironment and the contraction of the uterus, the main reactions for Zn and its alloys are the anodic oxidation of Zn and cathodic reduction of oxygen to form ZnO and Zn(OH)<sub>2</sub>, while the CaCO<sub>3</sub> (Fig. 9) might be the physical attachment from the uterus fluid calcification [28,33].

The  $\text{Cu}_2\text{O}$  is the main corrosion product formed on the surface of pure Cu when it is immersed in SUF for as long as 300 days. At the initial stage of soaking, the corrosion rate of pure Cu

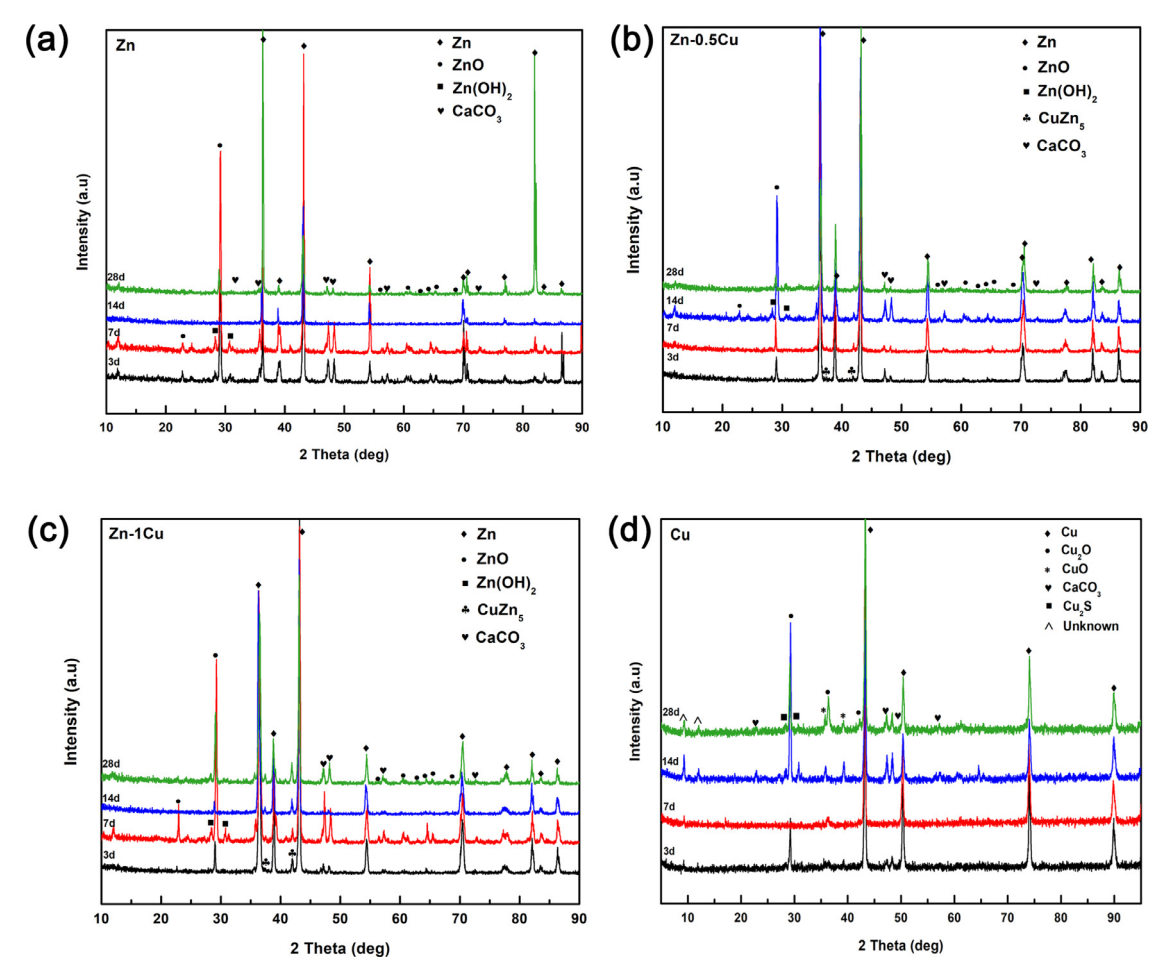


Fig. 9. XRD patterns for the (a) Zn, (b) Zn-05Cu, (c) Zn-1Cu and (d) Cu materials after implantation in rate uterine cavity for 3, 7, 14, and 28 days.

was higher than that of Zn alloy; It may be the initial  $\text{Cu}_2\text{O}$  attached to the surface of the Cu matrix that did not dissolve in the solution, resulting in the release of the initial  $\text{Cu}^{2+}$  is not as high as that of Zn. However, after 30 days, the corrosion rate of Zn alloys became higher than that of pure Cu and Zn. According to the electrochemical results, the corrosion current density and corrosion rate of the pure Cu were obviously higher than those of pure Zn. However, in the long-term soaking process, the dense cuprous oxide protective layer that was formed on the surface of pure Cu inhibited further corrosion of Cu, whereas the Zn alloy exhibited potential differences, and the galvanic corrosion accelerated the corrosion of Zn alloy due to the presence of the second phase  $\text{CuZn}_5$ .

# 4.2. Biocompatibility of Zn-Cu alloys in the uterine microenvironment

Zn, Zn-0.5Cu and Zn-1Cu presented much better biocompatibility than Cu from the *in vitro* and *in vivo* tests including cytotoxicity to two types of human endometrial cell (Fig. 6) and uterus cavity tissue compatibility (Fig. 7). Zn is the second most abundant metal element in the human body and plays a crucial role in the normal functions of the body by involving in ~300 types of biological enzymes reactions [51–54]. The long-term *in vitro* release rates of Zn<sup>2+</sup> from pure Zn, Zn-0.5Cu, and Zn-1Cu in SUF are much lower than the recommended daily intake value, 15 mg/d, for adults [55,56]. There is no systemic toxicity caused from Zn and its alloys implants. However, when the Zn and its alloys are implanted into the uterine cavity, locally high concentration of Zn<sup>2+</sup> from the corrosive degradation of the materials may result in toxic effects on

the cells or tissues [3,57,58]. Therefore, in this work we adopted two types of human endometrial cell lines, HEECs and HESCs that play an important role in the embryo implantation process [57,59–62], to evaluate the intrauterine cytotoxicity from Zn and allows

In vitro cytotoxicity results in Fig. 6 showed that the HEECs and HESCs cultured under high concentrations (100%) of pure Zn, Zn-0.5Cu, Zn-1Cu, and pure Cu materials extracts showed decreased cell viability and a certain degree of cytotoxicity compared with the control group, while cells treated with low concentrations (50% and 10%) of pure Zn, Zn-0.5Cu, and Zn-1Cu extracts showed no cytotoxicity. Moreover, the cell viability was improved to a certain extent, suggesting that the dose dependence on Zn and Cu may exist. The diluted extracts of Zn materials with higher cell viability agrees well with the recommended in vitro cytotoxicity evaluation criteria for biodegradable metals [63] and other reports on Zn alloys' cytotoxicity of different types of vascular cells [64,65]. A low concentration of Zn<sup>2+</sup> can improve cell viability and promote cell adhesion, migration, and proliferation, whereas a high concentration of Zn<sup>2+</sup> produces opposite effects, indicating the Zn<sup>2+</sup> concentration-dependent behaviour. We noticed that the cell viability of the both cells from the 10% extract of pure Cu group was higher on the first day; however, it decreased significantly with the extension of culture time. In addition, Zn-1Cu showed better cell viability than Zn-0.5Cu, which could be attributed to the bimodal antagonism from the low concentrations of Zn<sup>2+</sup> and high concentrations of Cu<sup>2+</sup> [66]. The pH values of the extracts did not exceed the normal pH range of the uterine fluid, 6.0~7.9 [67], sug-

gesting there is no chemcial effect on uterine fluid from Zn and alloys.

The issues of pain, abnormal uterine bleeding, and other adverse reactions associated with Cu-IUD have not been completely resolved yet [58,68]. Studies on the pathogenesis of adverse reactions have mainly focused on endometrial morphology [69] and changes in local biochemical substances in the uterus [70]. After Cu-IUD is implanted in the uterine cavity, it directly comes in contact with the endometrium and causes physical stimulation and mechanical compression of the endometrium [71]. In addition, Cu<sup>2+</sup> and corrosion products released into the uterine cavity by Cu-IUD can damage the endometrium and induce aseptic inflammation of the endometrium [72,73]. Notably, in the initial stage of Cu-IUD implantation, free Cu<sup>2+</sup> in the uterine cavity increases rapidly, which exerts a strong stimulation effect on the endometrium. Thus Cu-IUD-related adverse reactions usually occur at the initial stage of implantation.

For the *in vivo* tissue compatibility tests, we observed the endometrial morphological evolutions after Zn, Zn alloys and Cu implanted into uterine cavity using rat model. Analysis of endometrial changes at each time point of implantation indicated that the endometrial histomorphology changed to varying degrees with Zn and alloys implantation. With the increased implantation time, the stimulation of the endometrium gradually weakened and the endometrium gradually recovered. The histopathological observation results showed that the Zn-1Cu group exhibited excellent histocompatibility with slightest endometrial structure damage and the fastest recovery, followed by pure Zn, Zn-0.5Cu, and pure Cu. Because of the antagonistic effect of Cu<sup>2+</sup> and Zn<sup>2+</sup>, we speculate that Zn-1Cu has good biocompatibility, which may be related to the release of more Cu<sup>2+</sup> that may reduce the absorption of Zn<sup>2+</sup> by endometrial cells [66].

Analysis of changes in the corrosion surface of the materials at each time point of implantation revealed local corrosion on the surface of the three Zn materials. The corrosion products formed by local corrosion were relatively loose and showed a porous structure, which was conducive to the continuous release of Zn<sup>2+</sup> [74]. Simultaneously, no local corrosion of the surface was observed for pure Cu; hence, corrosion products were formed with the extension of implantation time, and the accumulation of these products could effectively protect the material matrix [75]. The structures formed by the two corrosion modes can reduce the explosive release of Zn<sup>2+</sup> in the initial stage of implantation and facilitate the release of Zn<sup>2+</sup> in the long-term implantation process. In addition, we observed the obvious peeling phenomenon of the corrosion products on the surface of pure Cu, which may be one of the reasons for poor histocompatibility.

### 5. Conclusions

Biodegradable Zn-Cu alloys exhibit a stable corrosion rate and a continuous Zn<sup>2+</sup> release in the simulated uterine microenvironment over 300 days, and great biocompatibility to cells and tissues. The Zn-Cu alloys also exert antifertility effect similar to pure Cu. The differences of the corrosion behaviours, pit corrosion for Zn and Zn-0.5/1Cu alloys and uniform surface corrosion for pure Cu, is the main reason for the improved burst release of the metallic ions in the initial days of immersion and implantation. Furthermore, the varied corrosion products formed on the surface of the Zn-Cu alloy with much more loose morphology could benefit the reduction of the explosive release of Zn<sup>2+</sup> and facilitate the release behaviour of Zn<sup>2+</sup> in the long-term process. Zn-Cu alloys exhibit the much more improved cell and tissue compatibility while maintain comparable antifertility efficiency, suggesting the Zn-Cu alloys could be substitution of Cu in the IUD, especially the Zn-1Cu alloy.

#### **Declaration of Competing Interest**

The authors declare no competing financial interests or personal relationships.

#### **CRediT authorship contribution statement**

**Guo Bao:** Conceptualization, Data curation, Formal analysis, Funding acquisition, Writing – original draft, Writing – review & editing. **Kun Wang:** Conceptualization, Data curation, Formal analysis, Formal analysis, Writing – original draft, Writing – review & editing. **Lijun Yang:** Data curation, Writing – original draft, Writing – review & editing. **Jialing He:** Formal analysis. **Bin He:** Conceptualization, Funding acquisition, Writing – review & editing. **Xiaoxue Xu:** Formal analysis, Writing – review & editing. **Yufeng Zheng:** Conceptualization, Funding acquisition, Writing – review & editing.

# Acknowledgements

This work was supported by National Natural Science Foundation of China (Grant No. 51931001 and 52171237), the National Key R&D Program of China (Grant No.2016YFC1000903), the Non-Profit Central Research Institute Fund of National Research Institute For Family Planning (Grant No. 2020GJZ07), CAMS Innovation Fund for Medical Sciences (CIFMS)(Grant No.2018-I2M-1-004).

# **Supplementary materials**

Supplementary material associated with this article can be found, in the online version, at doi:10.1016/j.actbio.2022.01.053.

#### References

- D.M. Bastidas, B. Valdez, M. Schorr, J.M. Bastidas, Corrosion of copper intrauterine devices: review and recent developments, Corros. Rev. 37 (2019) 307–320.
- [2] A.P. Carlos, F. Daniel, P. Eliane, D. Juan, B. Luis, The use of vaginal ultrasound to identify copper T IUDs at high risk of expulsion, Contraception 54 (1996) 287–289.
- [3] X.X. Xu, F.L. Nie, Y.B. Wang, J.X. Zhang, W. Zheng, L. Li, Y.F. Zheng, Effective inhibition of the early copper ion burst release with ultra-fine grained copper and single crystal copper for intrauterine device application, Acta Biomater. 8 (2012) 886–896.
- [4] A.T. Tita, J.M. Szychowski, K. Boggess, G. Saade, S. Longo, E. Clark, S. Esplin, K. Cleary, R. Wapner, K. Letson, M. Owens, A. Abramovici, N. Ambalavanan, G. Cutter, W. Andrews, C.S.T. Consortium, Adjunctive azithromycin prophylaxis for cesarean delivery, N. Engl. J. Med. 375 (2016) 1231–1241.
- [5] R. Lu, W. Ning, J. Zhao, Investigation of intrauterine microbes after intrauterine operation, Chin. J. Obstet. Gynecol. 33 (1998) 168.
- [6] T.M Farley, M.J. Rosenberg, P.J. Rowe, J.H. Chen, O. Meirik, Intrauterine device and pelvic inflammatory disease: an international perspective, Lancet 339 (1992) 785 -785.
- [7] P.A. O'Brien, R. Kulier, F.M. Helmerhorst, M. Usher-Patel, C. d'Arcangues, Copper-containing, framed intrauterine devices for contraception: a systematic review of randomized controlled trials, Contraception 77 (2008) 318–327.
- [8] J.Y. Liang, Y. Li, X. Gu, Y.L. Gao, J.P. Liu, Investigation of the release behavior of cupric ion for three types of Cu-IUDs and indomethacin for medicated Cu-IUD in simulated uterine fluid, Contraception 77 (2008) 299–302.
- [9] D. Allouche-Fitoussi, D. Bakhshi, H. Breitbart, Signaling pathways involved in human sperm hyperactivated motility stimulated by Zn<sup>2</sup>, Mol. Reprod. Dev. 85 (2018) 543–556.
- [10] E.C.S. Oliveira, M.R. Moura, V.A. Silva, C.A. Peixoto, K.L. Saraiva, M.J. de Sa, R.H. Douglas, A de Pinho Marques, Intratesticular injection of a zinc-based solution as a contraceptive for dogs, Theriogenology 68 (2007) 137–145.
- [11] E.C.S. Oliveira, A.K.F. Fagundes, C.C.S. Melo, L.T.B. Nery, Intratesticular injection of a zinc-based solution for contraception of domestic cats: a randomized clinical trial of efficacy and safety, Vet. J. 197 (2013) 307–310.
  [12] J.A. Zipper, H.J. Tatum, L. Pastene, M. Medel, M. Rivera, Metallic copper as an
- [12] J.A. Zipper, H.J. Tatum, L. Pastene, M. Medel, M. Rivera, Metallic copper as an intrauterine contraceptice adjunct to the "T" device, Am. J. Obstet. Gynecol. 105 (1969) 1274–1278.
- [13] J. Zipper, M. Medel, R. Prager, Supperssion of fertility by intrauterine copper, Am. J. Obst. Gynecol. 105 (1969) 529–534.
- [14] H.J. Tatum, Copper-bearing intrauterine devices, Clin. Obstet. Gynecol. 17 (1974) 93–119.
- [15] Z.H. Yang, C.S. Xie, X.P. Xia, S.Z Cai, Zn<sup>2+</sup> release behavior and surface characteristics of Zn/LDPE nanocomposites and ZnO/LDPE nanocomposites in simulated uterine solution, J. Mater. Sci. Mater. Med. 19 (2008) 3319–3326.

[16] Z.H. Yang, C.S. Xie, Zn<sup>2+</sup> release from zinc and zinc oxide particles in simulated uterine solution, Colloid Surf. B 47 (2006) 140–145.

- [17] X.H. Qu, H.T. Yang, B. Jia, Z.F. Yu, Y.F. Zheng, K.R. Dai, Biodegradable Zn-Cu alloys show antibacterial activity against MRSA bone infection by inhibiting pathogen adhesion and biofilm formation, Acta Biomater. 117 (2020) 400–417.
- [18] J.L. Niu, Z.B. Tang, H Huang, J Pei, H Zhang, G.Y. Yuan, W.J. Ding, Research on a Zn-Cu alloy as a biodegradable material for potential vascular stents application, Mater. Sci. Eng. C Mater. Biol. Appl. 69 (2016) 407–413.
- [19] I.M.W. Ebisch, C.M.G. Thomas, W.H.M. Peters, D.D.M. Braat, R.P.M. Steegers-Theunissen, The importance of folate, zinc and antioxidants in the pathogenesis and prevention of subfertility, Hum. Reprod. Update 13 (2007) 163–174.
- [20] L. Tulic, S. Vidakovic, I. Tulic, M. Curcic, Z. Bulat, Toxic metal and trace element concentrations in blood and outcome of *in vitro* fertilization in women, Biol. Trace Elem. Res. 188 (2019) 284–294.
- [21] Z.B. Tang, J.L. Niu, H. Huang, H. Zhang, J.M. Pei, J. Ou, G.Y. Yuan, Potential biodegradable Zn-Cu binary alloys developed for cardiovascular implant applications, J. Mech. Behav. Biomed. Mater. 72 (2017) 182–191.
- [22] C. Zhou, X.Y. Feng, Z.Z. Shi, C.X. Song, X.S. Cui, J.W. Zhang, T. Li, E.S. Toft, J.B. Ge, L.N. Wang, H.J. Zhang, Research on elastic recoil and restoration of vessel pulsatility of Zn-Cu biodegradable coronary stents, Biomed. Tech. (Berl.) 65 (2020) 219–227.
- [23] P.K. Bowen, E.R. Shearier, S. Zhao, R.J. Guillory, F. Zhao, J. Goldman, J.W. Drelich, Biodegradable metals for cardiovascular stents: from clinical concerns to recent Zn-alloys, Adv. Healthc. Mater. 5 (2016) 1121–1140.
- [24] H.T. Yang, C. Wang, C.Q. Liu, H.W. Chen, Y.F. Wu, J.T. Han, Z.C. Jia, W.J. Lin, D.Y. Zhang, W.T. Li, W. Yuan, H. Guo, H.F. Li, G.X. Yang, D.L. Kong, D.H. Zhu, K. Takashima, L.Q. Ruan, J.F. Nie, X. Li, Y.F. Zheng, Evolution of the degradation mechanism of pure zinc stent in the one-year study of rabbit abdominal aorta model. Biomaterials 145 (2017) 92–105.
- [25] P.K. Bowen, J. Drelich, J. Goldman, Zinc exhibits ideal physiological corrosion behavior for bioabsorbable stents, Adv. Mater. 25 (2013) 2577–2582.
- [26] H.T. Yang, B. Jia, Z.C. Zhang, X.H. Qu, G.N. Li, W.T. Lin, D.H. Zhu, K.R. Dai, Y.F. Zheng, Alloying design of biodegradable zinc as promising bone implants for load-bearing applications, Nat. Commun. 11 (2020) 401.
- [27] E. Mostaed, M. Sikora-Jasinska, J.W. Drelich, M. Vedani, Zinc-based alloys for degradable vascular stent applications, Acta Biomater. 71 (2018) 1–23.
- [28] H. Guo, D.D. Xia, Y.F. Zheng, Y. Zhu, Y.S. Liu, Y.S. Zhou, A pure zinc membrane with degradability and osteogenesis promotion for guided bone regeneration: *in vitro* and *in vivo* studies, Acta Biomater. 106 (2020) 396–409.
- [29] X. Liu, H.T. Yang, P. Xiong, W.T. Li, H.H. Huang, Y.F. Zheng, Comparative studies of Tris-HCl, HEPES and NaHCO3/CO2 buffer systems on the biodegradation behaviour of pure Zn in NaCl and SBF solutions, Corros. Sci. 157 (2019) 205–219.
- [30] Y. Chen, W. Zhang, M.F. Maitz, M. Chen, H. Zhang, J. Mao, Y. Zhao, N. Huang, G. Wan, Comparative corrosion behavior of Zn with Fe and Mg in the course of immersion degradation in phosphate buffered saline, Corros. Sci. 111 (2016) 541–555.
- [31] L.J. Liu, Y. Meng, C.F. Dong, Y. Yan, A.A. Volinsky, L.N. Wang, Initial formation of corrosion products on pure zinc in simulated body fluid, J. Mater. Sci. Technol. 34 (2018) 2271–2282.
- [32] L. Liu, Y. Meng, A.A. Volinsky, H.J. Zhang, L.N. Wang, Influences of albumin on *in vitro* corrosion of pure Zn in artificial plasma, Corros. Sci. 153 (2019) 341–356.
- [33] X. Liu, Y. Cheng, Z.P. Guan, Y.F Zheng, Exploring the effect of amino acid and glucose on the biodegradation of pure Zn, Corros. Sci. 170 (2020) 108661.
- [34] H. Guo, J.L. Hu, Z.Q. Shen, D.X. Du, Y.F. Zheng, J.R. Peng, *In vitro* and *in vivo* studies of biodegradable Zn-Li-Mn alloy staples designed for gastrointestinal anastomosis, Acta Biomater. 121 (2021) 713–723.
- [35] S.M. Chen, L.T. Yu, Q.Y. Zhao, Y.C. Ren, L.L. Guo, X.Y. Gong, X.J. Wan, G.Y. Yuan, B.W. Li, Comparative assessment of the biocompatibility and degradation behavior of Zn-3Cu and JDBM alloys used for biliary surgery, Am. J. Transl. Res. 12 (2020) 19–31.
- [36] S. Lin, X.L. Ran, X.H. Yan, L.Q Wang, J.G. Zhou, T.Z. Hu, G.X. Wang, Systematical evolution on a Zn-Mg alloy potentially developed for biodegradable cardiovascular stents, J. Mater. Sci. Mater. Med. 30 (2019) 122.
- [37] W. Pachla, S. Przybysz, A. Jarzebska, M. Bieda, K. Sztwiertnia, M. Kulczyk, J. Skiba, Structural and mechanical aspects of hypoeutectic Zn-Mg binary alloys for biodegradable vascular stent applications, Bioact. Mater. 6 (2021) 26–44.
- [38] R. Yue, J.L. Niu, Y.T. Li, G.Z. Ke, H. Huang, J. Pei, W.J. Ding, G.Y. Yuan, In vitro cy-tocompatibility, hemocompatibility and antibacterial properties of biodegradable Zn-Cu-Fe alloys for cardiovascular stents applications, Mater. Sci. Eng. C Mater. Biol. Appl. 113 (2020) 111007.
- [39] S.M. Zhu, C.C. Wu, G.N. Li, Y.F. Zheng, J.F. Nie, Microstructure, mechanical properties and creep behaviour of extruded Zn-xLi (x = 0.1, 0.3 and 0.4) alloys for biodegradable vascular, Mat. Sci. Eng. A Struct. 777 (2020) 139082.
- [40] H.T. Yang, X.H. Qu, W.J. Lin, C. Wang, D.H. Zhu, K.R. Dai, Y.F. Zheng, In vitro and in vivo studies on zinc-hydroxyapatite composites as novel biodegradable metal matrix composite for orthopedic applications, Acta Biomater. 71 (2018) 200–214.
- [41] B. Jia, H.T. Yang, Y. Han, Z.C. Zhang, X.H. Qu, Y.F. Zhuang, Q. Wu, Y.F. Zheng, K.R. Dai, *In vitro* and *in vivo* studies of Zn-Mn biodegradable metals designed for orthopedic applications, Acta Biomater. 108 (2020) 358–372.
- [42] P.S. Guo, X.L. Zhu, L.J. Yang, L. Deng, Q.K. Zhang, B.Q. Li, K. Cho, W.S. Sun, T.T. Ren, Z.L. Song, Ultrafine- and uniform-grained biodegradable Zn-0.5Mn alloy: grain refinement mechanism, corrosion behavior, and biocompatibility in vivo, Mater. Sci. Eng. C Mater. Biol. Appl. 118 (2021) 111391.

- [43] X.W. Liu, J.K. Sun, K.J. Qiu, Y.H. Yang, Z.J. Pu, L. Li, Y.F. Zheng, Effects of alloying elements (Ca and Sr) on microstructure, mechanical property and in vitro corrosion behavior of biodegradable Zn-1.5Mg alloy, J. Alloy. Compd. 664 (2016) 444–452.
- [44] D.H. Zhu, I. Cockerill, Y.C. Su, Z.X. Zhang, J.Y. Fu, K.W. Lee, J. Ma, C. Okpokwasili, L.P. Tang, Y.F. Zheng, Y.X. Qin, Y.D. Wang, Mechanical strength, biodegradation, and in vitro and in vivo biocompatibility of Zn biomaterials, ACS Appl. Mater. Interfaces 11 (2019) 6809–6819.
- [45] M.B. Kannan, C. Moore, S. Saptarshi, S. Somasundaram, M. Rahuma, A.L. Lopata, Biocompatibility and biodegradation studies of a commercial zinc alloy for temporary mini-implant applications, Sci. Rep. 7 (2017) 15605.
- [46] G. Bao, Q.Q. Fan, D.F. Ge, K. Wang, M.M. Sun, Z.C. Zhang, H. Guo, H.T. Yang, B. He, Y.F. Zheng, *In vitro* and *in vivo* studies to evaluate the feasibility of Zn-0.1Li and Zn-0.8Mg application in the uterine cavity microenvironment compared to pure zinc, Acta Biomater. 123 (2021) 393–406.
- [47] ASTM G31-72, Standard Practice for Laboratory Immersion Corrosion Testing of Metals, ASTM International, Philadelphia West Conshohocken, PA, 2004.
- [48] ASTM G1-03 Standard Practice for PreparingCleaning, and Evaluating Corrosion Test Specimens, ASTM International, Philadelphia West Conshohocken, PA, 2004
- [49] K. Wang, G. Bao, Q.Q. Fan, L.Q. Zhu, L.J. Yang, T.T. Liu, Z.C. Zhang, G.N. Li, X.H. Chen, X.X. Xu, X.B. Xu, B. He, Y.F. Zheng, Feasibility evaluation of a Cu-38 Zn alloy for intrauterine devices: in vitro and in vivo studies, Acta Biomater. 138 (2022) 561–575. ISSN 1742-7061.
- [50] M. Mouanga, P. Berçot, Comparison of corrosion behaviour of zinc in NaCl and in NaOH solutions; Part II: Electrochemical analyses, Corros. Sci. 52 (2010) 3993–4000
- [51] A.S. Prasad, B. Bao, Molecular mechanisms of Zinc as a pro-antioxidant mediator: clinical therapeutic implications, Antioxid. (Basel) 8 (2019) 164.
- [52] A.S. Prasad, Clinical, immunological, anti-inflammatory and antioxidant roles of zinc, Exp. Gerontol. 43 (2008) 370–377.
- [53] L. Rink, P. Gabriel, Zinc and the immune system, Proc. Nutr. Soc. 59 (2000) 541–552.
- [54] J.E. Coleman, Zinc proteins: enzymes, storage proteins, transcription factors, and replication proteins, Annu. Rev. Biochem. 61 (1992) 897–946.
- [55] C. Ogino, G.Y. Yang, Requirement of Rainbow Trout for Dietary Zinc, Bull. Jpn. Soc. Sci. Fish. 44 (1978) 1015–1018.
- [56] H. Tapiero, K.D. Tew, Trace elements in human physiology and pathology: zinc and metallothioneins, Biomed. Pharmacother. 57 (2003) 399–411.
- [57] J.P. Carrascosa, D. Cotán, I. Jurado, M. Oropesa-Ávila, P. Sánchez-Martín, R.F. Savarís, J. Tan, J.A. Sánchez-Alcázar, S.L. Tan, J.A. Horcajadas, The effect of copper on endometrial receptivity and induction of apoptosis on decidualized human endometrial stromal cells, Reprod. Sci. 25 (2017) 985–999.
- [58] D.M. Bastidas, B. Valdez, M. Schorr, J.M. Bastidas, Corrosion of copper intrauterine devices: review and recent developments, Corros. Rev. 37 (2019) 307–320.
- [59] K.N. Khan, A. Fujishita, M. Kitajima, K. Hiraki, M. Nakashima, H. Masuzaki, Intra-uterine microbial colonization and occurrence of endometritis in women with endometriosis, Hum. Reprod. 29 (2014) 2446–2456.
- [60] R. Azizi, L. Aghebati-Maleki, M. Nouri, F. Marofi, S. Negargar, M. Yousefi, Stem cell therapy in asherman syndrome and thin endometrium: stem cell- based therapy, Biomed. Pharmacother. 102 (2018) 333–343.
- [61] D. Wildemeersch, E. Schacht, Endometrial suppression with a new 'frameless' levonorgestrel releasing intrauterine system in perimenopausal and postmenopausal women: a pilot study, Maturitas 36 (2000) 63–68.
- [62] D. Wildemeersch, D. Janssens, E. Schacht, K. Pylyser, N. de Wever, Intrauterine levonorgestrel delivered by a frameless system, combined with systemic estrogen: acceptability and endometrial safety after 3 years of use in peri- and postmenopausal women, Gynecol. Endocrinol. 20 (2005) 336–342.
- [63] J.L. Wang, F. Witte, T.F. Xi, Y.F. Zheng, K. Yang, Y.S. Yang, D.W. Zhao, J. Meng, Y.D. Li, W.R. Li, K.M. Chan, L. Qin, Recommendation for modifying current cyto-toxicity testing standards for biodegradable magnesium-based materials, Acta Biomater. 21 (2015) 237–249.
- [64] E.R. Shearier, P.K. Bowen, W.L. He, A. Drelich, J. Drelich, J. Goldman, F. Zhao, *In vitro* cytotoxicity, adhesion, and proliferation of human vascular cells exposed to zinc, ACS Biomater. Sci. Eng. 2 (2016) 634–642.
- [65] J. Ma, N. Zhao, D.H. Zhu, Endothelial cellular responses to biodegradable metal zinc, ACS Biomater. Sci. Eng. 1 (2015) 1174–1182.
- [66] J. Wu, L.Y. Wang, J. He, C.H. Zhu, In vitro cytotoxicity of Cu<sup>2+</sup>, Zn<sup>2+</sup>, Ag<sup>+</sup> and their mixtures on primary human endometrial epithelial cells, Contraception 85 (2012) 509–518.
- [67] L.G. Feo, The pH of the human uterine cavity *in situ*, Am. J. Obstet. Gynecol. 70 (1955) 60–64.
- [68] D. Wildemeersch, A. Andrade, N. Goldstuck, Femilis® 60 levonorgestrel-releasing intrauterine system-a review of 10 years of clinical experience, Clin. Med. Insights Reprod. Health 10 (2016) 19–27.
- [69] X.P. Xia, C.S. Xie, C.H. Zhu, S.Z. Cai, X.L. Yang, Effect of implanted Cu/low-density polyethylene nanocomposite on the morphology of endometrium in the mouse, Fertil. Steril. 88 (2007) 472–478.
- [70] J. Lee, S.K. Banu, T. Subbarao, A. Starzinski-Powitz, J.A. Arosh, Selective inhibition of prostaglandin E2 receptors EP2 and EP4 inhibits invasion of human immortalized endometriotic epithelial and stromal cells through suppression of metalloproteinases, Mol. Cell Endocrinol. 332 (2011) 306–312
- [71] K. Patai, I. Balogh, Z. Szarvas, Clinicopathological problems of the local tissue effect of the copper-releasing intrauterine contraceptive device (IUD). I.

- General characteristics of the copper-containing IUD (clinical study), Acta Chir.
- General characteristics of the copper-containing IUD (clinical study), Acta Chir. Hung. 30 (1989) 129–132.
  [72] E. Johannisson, Mechanism of action of intrauterine devices: biochemical changes, Contraception 36 (1987) 11–22.
  [73] G. Grasso, M. Muscettola, V. Bocci, The physiological interferon response. I. Cells attached to intrauterine devices release interferon *in vitro*, Proc. Soc. Exp. Biol. Med. 173 (1983) 276–280.
- [74] P. Li, J.T. Dai, E. Schweizer, F. Rupp, A. Heiss, A. Richter, U.E. Klotz, J. Geis-Gerstorfer, L. Scheideler, D. Alexander, Response of human periosteal cells to degradation products of zinc and its alloy, Mater. Sci. Eng. C Mater. Biol. Appl. 108 (2020) 110208.
- [75] T.H. Muster, I.S. Cole, The protective nature of passivation films on zinc: surface charge, Corros. Sci. 46 (2004) 2319–2335.